Dynamics of cylindrical domain walls in nematic liquid crystals

Joachim Stelzer and Henryk Arodź

Instytut Fizyki, Uniwersytet Jagielloński, Reymonta 4, 30-059 Kraków, Poland

(May 25, 2022)

Abstract

Analytical calculations of the dynamics of a curved domain wall in a nematic liquid crystal are performed. The core of the wall is assumed to form a cylinder, whose axis coincides with the direction of an external magnetic field. The equation of motion for the nematic director field is solved in a comoving coordinate frame by applying a polynomial expansion of the tilt angle with respect to the radial distance from the wall core. Starting from a cylindrical domain wall at rest as initial conditions, the shrinking of the cylinder and the change of the wall width is analysed in detail. In particular, we find that the Néel wall decays faster than the Bloch wall, in agreement with energy considerations.

PACS: 61.30.Jf, 11.27.+d

Typeset using REVTEX

I. INTRODUCTION

It is a well-known fact that nematic liquid crystals reveal a large variety of defect structures. Such defects are very interesting from the theoretical point of view [1–3]. Moreover, they are important for applications, *e.g.*, they play an crucial rôle in the switching mechanisms in modern liquid crystal display devices (surface-stabilized ferroelectric liquid crystal cells) [4–7]. Therefore, a quantitative investigation of defect dynamics is desirable.

The types of defects in the nematic director field cover zero- and one-dimensional objects (point and line defects, respectively) that arise due to the presence of impurities or surfaces [3,8]. Two-dimensional sheets, *i.e.* walls, are unstable in an isolated nematic. They can be stabilized, however, by imposing an external magnetic field [9]. The situation is similar to domain walls in a ferromagnetic material where regions of different spin orientations are separated by a thin boundary layer [10]. In a nematic, the director can align parallel or antiparallel to the external magnetic field. Due to fact that the director "lacks the arrowhead", these two situations are energetically equivalent. It may happen, that two spatial regions of antiparallel director orientation will form, with a domain wall between them [9].

Domain walls in nematics due to the existence of an external field are static in a planar geometry [9]. A qualitatively new behaviour occurs, when the shape of the wall is curved. In this case the wall becomes a dynamical object, *i.e.* its core starts to move, whereas the wall width is changing. The present paper is devoted to a quantitative study of the dynamics of domain walls in a cylindrical geometry. We consider the case of director reorientation through a Bloch and Néel wall [11,12]. From a methodological point of view, in our calculations we use the so-called *polynomial approximation* – it has turned out to be very fruitful in studies of defect dynamics in relativistic scalar field theories [13]. Due to the cylindrical symmetry, we can find explicit analytical solutions to equations of motion obtained within that approximation.

The organization of the paper is as follows. In section II the equation of motion for the director field is derived on the basis of the Ericksen-Leslie theory [14,15] for the case of a cylindrical domain wall of Bloch or Néel type in a nematic liquid crystal. Section III develops the polynomial expansion as an analytical method to solve approximately the dynamics of the director field. Within this approach, we obtain closed expressions for the dynamics of the wall core and width. In section IV some selected results together with their discussion are presented. Section V contains an outlook on possible extensions of our investigations.

II. DIRECTOR EQUATIONS OF MOTION FOR CYLINDRICAL DOMAIN WALLS

A. Comoving polar coordinates

For all calculations we restrict ourselves to the cylindrical geometry as pointed out in Figs. 1 and 2. The cylinder axis is determined by the orientation of the external magnetic field $\boldsymbol{H}$ which coincides with the z-axis of our coordinate frame, *i.e.* $\boldsymbol{H} = H_0\,\hat{\boldsymbol{z}}$. ($\hat{\boldsymbol{z}}$ denotes the unit vector along z.) As already mentioned above, a domain wall occurs for parallel and antiparallel director orientation with respect to the external field in different spatial regions. In the case of axial geometry, we assume the director to be aligned along the positive or negative z-axis (*up, down*) inside or outside the cylinder, respectively. Now the director can reorient from *up* to *down* in either $\hat{\boldsymbol{\phi}} - \hat{\boldsymbol{z}}-$plane or $\hat{\boldsymbol{\rho}} - \hat{\boldsymbol{z}}-$plane, where (ρ, ϕ, z) are cylindrical coordinates. We refer to these two cases as *Bloch* (Fig. 1) and *Néel* (Fig. 2) wall, taking over the nomenclature from planar domain walls in ferromagnetics [10] and nematics [9].

For our calculations it will be advantageous to work within a comoving cylindrical coordinate frame. The radial coordinate consists of the wall radius $\rho(t)$ and the radial distance ξ from the wall. These are related to cartesian coordinates according to

$$x = (\rho(t) + \xi)\,\cos\phi, \qquad y = (\rho(t) + \xi)\,\sin\phi. \tag{1}$$

The Nabla operator, expressed in the comoving coordinates, reads

$$\boldsymbol{\nabla} = \hat{\boldsymbol{\xi}}\,\frac{\partial}{\partial \xi} + \hat{\boldsymbol{\phi}}\,\frac{1}{\rho+\xi}\,\frac{\partial}{\partial \phi} + \hat{\boldsymbol{z}}\,\frac{\partial}{\partial z}. \tag{2}$$

The "spatial" time derivative $\partial\ /\partial t$ is related to the "material" (*i.e.* comoving) time derivative $D\ /Dt$ by the chain rule between the coordinate sets $x_i = (x, y, z)$ and $\xi_\alpha = (\xi, \phi, z)$ (laboratory and comoving coordinates):

$$\frac{\partial}{\partial t} = \frac{D}{Dt} - \left.\frac{\partial x_i}{\partial t}\right|_{\xi_\alpha} \frac{\partial \xi_\alpha}{\partial x_i}\,\frac{\partial}{\partial \xi_\alpha}. \tag{3}$$

The relation above is simplified for cylindrical geometry

$$\frac{\partial}{\partial t} = \frac{D}{Dt} - \dot{\rho}\,\frac{\partial}{\partial \xi}. \tag{4}$$

For the Bloch and Néel wall we can describe the director orientation by the *tilt angle field* $\Theta(\xi, t)$ which measures the angle between the local director and the z-axis. In terms of the comoving frame, the director is in the $\hat{\boldsymbol{\phi}}-\hat{\boldsymbol{z}}-$plane for the Bloch wall and in the $\hat{\boldsymbol{\xi}}-\hat{\boldsymbol{z}}-$plane for the Néel wall:

$$\boldsymbol{n}_B = \sin\Theta(\xi, t)\,\hat{\boldsymbol{\phi}}(\phi, t) + \cos\Theta(\xi, t)\,\hat{\boldsymbol{z}}, \qquad \text{(Bloch wall)} \tag{5}$$

$$\boldsymbol{n}_N = \sin\Theta(\xi, t)\,\hat{\boldsymbol{\xi}}(\phi, t) + \cos\Theta(\xi, t)\,\hat{\boldsymbol{z}}. \qquad \text{(Néel wall)} \tag{6}$$

B. Free energy density

In the framework of the Ericksen-Leslie theory [14,15] the dynamics of the director field follows from the balance between elastic, magnetic and viscous torques. The latter are determined by the temporal change in the director, whereas elastic and magnetic torques are obtained as a variational derivative from a free energy density $\mathcal{F}$. Thus the equation of motion for the director components generally reads

$$\gamma_1\,\frac{\partial n_i}{\partial t} = -\frac{\delta \mathcal{F}}{\delta n_i} \equiv \partial_j\,\frac{\partial \mathcal{F}}{\partial(\partial_j n_i)} - \frac{\partial \mathcal{F}}{\partial n_i}. \tag{7}$$

In Eq. (7) γ_1 is the rotational viscosity of the liquid crystal. In fact, Eq. (7) should contain an additional term λn_i, with the Lagrange multiplier λ, accounting for the constraint of

$\boldsymbol{n}$ being a unit vector. In the cylindrical geometry under consideration, however, it turns out, that this constraint can be incorporated much more easily by starting from (7) (*i.e.* without the Lagrange multiplier). Later on we shall eliminate the variation of the length of the director by taking appropriate projections, as will be demonstrated below.

The free energy density $\mathcal{F}$ consists of an elastic and a magnetic part ($\mathcal{F} = \mathcal{F}_{\text{elast}} + \mathcal{F}_{\text{mag}}$). For the elastic free energy density we take the Oseen-Zöcher-Frank expression [16–18], that contains *splay*, *twist* and *bend* deformations of the director field.

$$\mathcal{F}_{\text{elast}} = \frac{1}{2}\, K_{11}\, (\operatorname{div} \boldsymbol{n})^2 + \frac{1}{2}\, K_{22}\, (\boldsymbol{n} \cdot \operatorname{curl} \boldsymbol{n})^2 + \frac{1}{2}\, K_{33}\, (\boldsymbol{n} \times \operatorname{curl} \boldsymbol{n})^2. \tag{8}$$

In (8) K_{11}, K_{22} and K_{33} denote elastic constants of the nematic liquid crystal.

The magnetic free energy density couples the director $\boldsymbol{n}$ to the magnetic field $\boldsymbol{H}$ via the anisotropy of the magnetic susceptibility $\Delta\chi$ (μ_0 means the magnetic field constant).

$$\mathcal{F}_{\text{mag}} = -\frac{1}{2}\, \mu_0\, \Delta\chi\, (\boldsymbol{n} \cdot \boldsymbol{H})^2. \tag{9}$$

For a cylindrical Bloch or Néel wall we can express the free energy density explicitly in comoving coordinates,

$$\begin{aligned}
\mathcal{F}_B &= \frac{1}{2}\, K_{22} \left(\Theta' + \frac{\cos\Theta\, \sin\Theta}{\rho + \xi} \right)^2 + \frac{1}{2}\, K_{33}\, \frac{\sin^4\Theta}{(\rho+\xi)^2} \\
&\quad - \frac{1}{2}\, \mu_0\, \Delta\chi\, H_0^2\, \cos^2\Theta, \qquad \text{(Bloch wall)} && (10) \\
\mathcal{F}_N &= \frac{1}{2}\, K_{11} \left(\Theta' \cos\Theta + \frac{\sin\Theta}{\rho + \xi} \right)^2 + \frac{1}{2}\, K_{33}\, \Theta'^{\,2}\, \sin^2\Theta \\
&\quad - \frac{1}{2}\, \mu_0\, \Delta\chi\, H_0^2\, \cos^2\Theta. \qquad \text{(Néel wall)} && (11)
\end{aligned}$$

In (10) and (11) Θ' stands for the radial derivative $\partial\Theta/\partial\xi$.

C. Director equation of motion

Returning to Eq. (7) we now have to account for the constraint of the director normalization ($|\boldsymbol{n}| = 1$). To this aim we write the left-hand side (LHS) of (7) explicitly in comoving coordinates.

$$\mathrm{LHS}_B = -\gamma_1\,(\dot\Theta - \dot\rho\,\Theta')\,(\hat{\boldsymbol{\xi}}\times\boldsymbol{n}), \qquad \text{(Bloch wall)} \tag{12}$$

$$\mathrm{LHS}_N = \gamma_1\,(\dot\Theta - \dot\rho\,\Theta')\,(\hat{\boldsymbol{\phi}}\times\boldsymbol{n}). \qquad \text{(Néel wall)} \tag{13}$$

Here $\dot\Theta$ denotes the material time derivative $D\Theta/Dt$.

For further considerations we express the right-hand side (RHS) of (7) in cartesian coordinates. Its components read

$$\begin{aligned}\mathrm{RHS}_i = {} & K_{11}\,\partial_i\,(\mathrm{div}\,\boldsymbol{n}) - K_{22}\,(\boldsymbol{n}\cdot\mathrm{curl}\,\boldsymbol{n})\,(\mathrm{curl}\boldsymbol{n})_i\\ & -K_{22}\,\{\mathrm{curl}\,[(\boldsymbol{n}\cdot\mathrm{curl}\boldsymbol{n})\,\boldsymbol{n}]\}_i\\ & -K_{33}\,\{(n_k\,\partial_k n_j)\,\partial_i n_j - \partial_k[n_k(n_j\,\partial_j n_i)]\}\\ & +\mu_0\,\Delta\chi\,(\boldsymbol{n}\cdot\boldsymbol{H})\,H_i.\end{aligned} \tag{14}$$

The constraint of the director normalization $|\boldsymbol{n}| = 1$ means that we have to discard the (infinitesimal) variation of the length of the director $\delta\boldsymbol{n} = \epsilon(\boldsymbol{r})\,\boldsymbol{n}$. ($\epsilon(\boldsymbol{r})$ is a small number everywhere.) The corresponding variation of the total free energy F (which is the volume integral over the free energy density $\mathcal{F}$) reads

$$\delta F = \int \mathrm{d}^3r\,\frac{\delta\mathcal{F}}{\delta\boldsymbol{n}}\cdot\delta\boldsymbol{n} = \int \mathrm{d}^3r\,\epsilon(\boldsymbol{r})\,\boldsymbol{n}\cdot\frac{\delta\mathcal{F}}{\delta\boldsymbol{n}} = 0. \tag{15}$$

From Eq. (15) it is obvious that *the variation of the director length is related to the projection of the variational derivative of the free energy density* (*i.e.* of the RHS (14)) *onto the director.* Moreover, from (12), (13) we recognize that the LHS, projected onto the director, yields zero. Thus we conclude that by discarding the projection of Eq. (7) onto the director we properly take into account the director constraint!

Additionally, after some lengthy calculations we find that for the Bloch and Néel wall the projection onto $\hat{\boldsymbol{\xi}}$ and $\hat{\boldsymbol{\phi}}$, respectively, yield identically zero. Thus the scalar equation of motion for the tilt angle field $\Theta(\xi, t)$ can be obtained by projecting (7) onto the the third linearly independent direction, which is $(\hat{\boldsymbol{\xi}}\times\boldsymbol{n})$ for the Bloch wall and $(\hat{\boldsymbol{\phi}}\times\boldsymbol{n})$ for the Néel wall. After performing the projections and changing for the comoving coordinates, we obtain the equations of motion for the tilt angle field.

$$
\begin{aligned}
\gamma_1\,(\dot\Theta - \dot\rho\,\Theta') = {} & K_{22}\,\Theta'' + K_{22}\,\frac{\Theta'}{\rho+\xi} \\
& - K_{22}\,\frac{\sin\Theta\,\cos\Theta}{(\rho+\xi)^2} \\
& - 2\,(K_{33}-K_{22})\,\frac{\cos\Theta\,\sin^3\Theta}{(\rho+\xi)^2} \\
& - \mu_0\,\Delta\chi\,H_0^2\,\sin\Theta\,\cos\Theta, \qquad \text{(Bloch wall)}
\end{aligned} \tag{16}
$$

$$
\begin{aligned}
\gamma_1\,(\dot\Theta - \dot\rho\,\Theta') = {} & K_{11}\,\cos\Theta\,\frac{\partial}{\partial\xi}\left\{\frac{1}{\rho+\xi}\,\frac{\partial}{\partial\xi}\,[(\rho+\xi)\,\sin\Theta]\right\} \\
& - K_{33}\,\sin\Theta\,\frac{\partial}{\partial\xi}\left\{\frac{1}{\rho+\xi}\,\frac{\partial}{\partial\xi}\,[(\rho+\xi)\,\cos\Theta]\right\} \\
& - K_{33}\,\frac{\sin\Theta\,\cos\Theta}{(\rho+\xi)^2} \\
& - \mu_0\,\Delta\chi\,H_0^2\,\sin\Theta\,\cos\Theta. \qquad \text{(Néel wall)}
\end{aligned} \tag{17}
$$

In agreement with the pictorial visualization of Figs. 1 and 2 the cylindrical Bloch wall contains no *splay* deformations, whereas in the Néel wall *twist* deformations are absent.

III. SOLUTION FOR THE DIRECTOR DYNAMICS

A. Polynomial expansion

The method to construct an approximate solution of the equations of motion (16), (17) is the *polynomial expansion of the field* which has been developed in previous papers [13]. We shall specify it here to the case of cylindrical domain walls in nematic liquid crystals.

The key idea is to take the spatial dependence of the tilt angle field $\Theta(\xi, t)$ as a Taylor-like expansion with respect to the wall distance ξ around its "core" value $\Theta(\xi = 0,\, t)$. The wall core corresponds to the radius of the cylinder (*i.e.* $\xi = 0$), where the director is oriented perpendicular to the z-axis, thus $\Theta(\xi = 0,\, t) = \frac{\pi}{2}\ \forall t$. The temporal evolution of the field is governed by the expansion coefficients.

$$
\Theta(\xi, t) = \frac{\pi}{2} + a(t)\,\xi + \frac{1}{2}\,b(t)\,\xi^2 + \frac{1}{6}\,c(t)\,\xi^3. \tag{18}
$$

The polynomial expansion cannot be truncated at arbitrary order, because we have to glue the bulk solution for $\Theta(\xi, t)$ smoothly to the boundary conditions. This is not always possible. However, it has been demonstrated for the case of cylindrical domain walls in a relativistic field theory (where the same symmetry considerations are valid as in our case), that the third-order polynomial expansion (18) guarantees the compatibility of the bulk solution with the boundary conditions [13]. Of course, for higher order of the Taylor expansion the accuracy of the calculations will increase.

From (18) we can easily obtain the spatial and temporal derivatives of the tilt angle field $\Theta(\xi, t)$. The trigonometric and fractional expressions that occur in the equations of motion (16), (17) are expanded as well up to third order in the wall distance ξ. All these expansions are then inserted into (16) and (17). By comparison of the coefficients of subsequent orders in ξ we obtain a set of ordinary differential equations for the expansion coefficients $a(t)$, $b(t)$ and $c(t)$. For the third-order polynomial expansion (18) such a comparison yields meaningful results for zeroth and first order in ξ. Thus from our calculations we obtain two equations that read as follows:

$$\gamma_1\, \dot{\rho}\, a = -K_{22}\, b - K_{22}\, \frac{a}{\rho}, \qquad \text{(Bloch wall)} \tag{19}$$

$$\begin{aligned} \gamma_1\, (\dot{a} - \dot{\rho}\, b) = {} & K_{22}\, c + K_{22}\, \frac{b}{\rho} + 2\,(K_{33} - K_{22})\, \frac{a}{\rho^2} \\ & + \mu_0\, \Delta\chi\, H_0^2\, a, \qquad \text{(Bloch wall)} \end{aligned} \tag{20}$$

$$\gamma_1\, \dot{\rho}\, a = -K_{33}\, b - K_{33}\, \frac{a}{\rho}, \qquad \text{(Néel wall)} \tag{21}$$

$$\begin{aligned} \gamma_1\, (\dot{a} - \dot{\rho}\, b) = {} & K_{33}\, c + K_{33}\, \frac{b}{\rho} \\ & -(K_{33} - K_{11})\, \frac{a}{\rho^2} - (K_{33} - K_{11})\, a^3 \\ & + \mu_0\, \Delta\chi\, H_0^2\, a. \qquad \text{(Néel wall)} \end{aligned} \tag{22}$$

B. Boundary conditions

Next we have to incorporate the boundary conditions. These are determined by the director alignment parallel and antiparallel to the external magnetic field inside and outside the wall, respectively. The (instantaneous) wall thickness is given as $\xi_0(t) + \xi_1(t)$, where

$\xi_0(t)$ measures the outward distance from the core to the outer edge of the wall, whereas $\xi_1(t)$ means the core-to-edge distance towards the cylinder axis. Therefore the boundary conditions read

$$\Theta(\xi_0, t) = \pi, \qquad \Theta(-\xi_1, t) = 0, \tag{23}$$

$$\Theta'(\xi_0, t) = 0, \qquad \Theta'(-\xi_1, t) = 0. \tag{24}$$

Eqs. (23) determine the director orientation at the edge of the wall, and Eqs. (24) are the conditions for the smoothness of the solution.

We can immediately express the boundary conditions in terms of the polynomial expansion for the tilt angle field (18):

$$a\,\xi_0 + \tfrac{1}{2}\,b\,\xi_0^2 + \tfrac{1}{6}\,c\,\xi_0^3 = \tfrac{\pi}{2}, \tag{25}$$

$$a + b\,\xi_0 + \tfrac{1}{2}\,c\,\xi_0^2 = 0, \tag{26}$$

$$-a\,\xi_1 + \tfrac{1}{2}\,b\,\xi_1^2 - \tfrac{1}{6}\,c\,\xi_1^3 = -\tfrac{\pi}{2}, \tag{27}$$

$$a - b\,\xi_1 + \tfrac{1}{2}\,c\,\xi_1^2 = 0. \tag{28}$$

The equations above form a set of inhomogeneous linear equations for the expansion coefficients $a(t)$, $b(t)$, $c(t)$. The solubility conditions yield relations between the expansion coefficients and the wall partial widths $\xi_0(t)$ and $\xi_1(t)$.

$$\xi_0 = \xi_1, \qquad a = \frac{3\pi}{4\xi_0}, \tag{29}$$

$$b = 0, \qquad c = -\tfrac{3\pi}{2\xi_0^3} = -\tfrac{32}{9\pi^2}\,a^3. \tag{30}$$

We note that the partial widths of the wall have turned out identical, and that there is no quadratic term in the polynomial expansion.

These relations must hold also in the bulk equations (19)–(22) in order to fulfill the boundary conditions. Introducing them, (19)–(22) become simplified.

$$\gamma_1\,\dot\rho = -\frac{K_{22}}{\rho}, \qquad \text{(Bloch wall)} \tag{31}$$

$$\gamma_1\,\dot a = -\tfrac{32}{9\pi^2}\,K_{22}\,a^3 + 2\,(K_{33} - K_{22})\,\frac{a}{\rho^2}$$

$$+\mu_0\,\Delta\chi\,H_0^2\,a, \qquad \text{(Bloch wall)} \tag{32}$$

$$\gamma_1\,\dot\rho = -\frac{K_{33}}{\rho}, \qquad \text{(Néel wall)} \tag{33}$$

$$\gamma_1\,\dot a = -(\tfrac{32}{9\pi^2}\,K_{33} + K_{33} - K_{11})\,a^3 - (K_{33} - K_{11})\,\frac{a}{\rho^2}$$

$$+\mu_0\,\Delta\chi\,H_0^2\,a. \qquad \text{(Néel wall)} \tag{34}$$

Equations (31) and (33) describe the time evolution of the wall core, *i.e.* the cylinder radius, whereas (32) and (34) govern the dynamics of the wall half-width, for the Bloch and Néel wall, respectively.

C. Solution for the wall dynamics

The coupled equations of motion (31)–(34) can be solved analytically. First we solve (31) and (33) for the dynamics of the wall core. It obeys a square root law:

$$\rho(t) = = \sqrt{\rho_0^2 - 2\,\frac{K_{22}}{\gamma_1}\,t}, \qquad \text{(Bloch wall)} \tag{35}$$

$$\rho(t) = = \sqrt{\rho_0^2 - 2\,\frac{K_{33}}{\gamma_1}\,t}. \qquad \text{(Néel wall)} \tag{36}$$

Qualitatively, starting from a wall radius ρ_0, the cylindrical domain wall will shrink. This behaviour is similar to what has been found for relativistic field theories [13]. For usual nematics K_{22} is the smallest of the elastic constants. Therefore the (35) and (36) indicate that the decay time of the Bloch wall is larger than that of the Néel wall.

Now we can use the solutions (35), (36) to eliminate the ρ-dependence from the equations of motion for the wall width (32), (34). The latter then read

$$\dot a = A(t)\,a - B\,a^3, \tag{37}$$

where the abbreviations stand for

$$A(t) = \frac{2\,(K_{33} - K_{22})}{\gamma_1\,\rho_0^2 - 2\,K_{22}\,t} + \frac{\mu_0\,\Delta\chi}{\gamma_1}\,H_0^2, \qquad \text{(Bloch wall)} \tag{38}$$

$$B = \tfrac{32}{9\pi^2}\,\frac{K_{22}}{\gamma_1}, \qquad \text{(Bloch wall)} \tag{39}$$

$$A(t) = -\frac{(K_{33} - K_{11})}{\gamma_1\, \rho_0^2 - 2\, K_{33}\, t} + \frac{\mu_0\, \Delta\chi}{\gamma_1}\, H_0^2, \qquad \text{(Néel wall)} \tag{40}$$

$$B = \tfrac{32}{9\pi^2}\, \frac{K_{33}}{\gamma_1} + \frac{K_{33} - K_{11}}{\gamma_1}. \qquad \text{(Néel wall)} \tag{41}$$

Eq. (37) is an ordinary differential equation of Bernoulli type. By the substitution $a = 1/\sqrt{\tilde{a}}$ it can be transformed into an inhomogeneous linear differential equation

$$\dot{\tilde{a}} + 2\, A(t)\, \tilde{a} = 2\, B, \tag{42}$$

whose general solution is obtained from a two-fold integration:

$$\tilde{a}(t) = \frac{1}{M(t)}\, [2\, B\, N(t) + \tilde{a}_0], \tag{43}$$

$$M(t) = \exp(\int_0^t \mathrm{dt'}\, 2\, \mathrm{A(t')}), \tag{44}$$

$$N(t) = \int_0^t \mathrm{d}t'\, M(t'). \tag{45}$$

$\tilde{a}_0$ is the initial value for the auxiliary variable $\tilde{a}(t)$. This variable is related closely to the wall half-width $\xi_0(t)$ (Eq.(51) below).

For our case of the cylindrical domain walls all integrals can be solved analytically.

$$M(t) = \mathrm{e}^{\alpha\, t}\, (1 - \beta\, t)^{\delta}, \tag{46}$$

$$N(t) = \frac{\mathrm{e}^{\alpha/\beta}}{\beta}\, \left(\frac{\beta}{\alpha}\right)^{\delta+1}\, \left[\gamma(\delta+1, \frac{\alpha}{\beta}) - \gamma(\delta+1, \frac{\alpha}{\beta} - \alpha\, t)\right], \tag{47}$$

where further abbreviations are introduced:

$$\alpha = \frac{2\, \mu_0\, \Delta\chi}{\gamma_1}\, H_0^2, \quad \beta = \frac{2\, K_{22}}{\gamma_1\, \rho_0^2}, \quad \delta = -2\, \frac{K_{33}}{K_{22}} + 2, \qquad \text{(Bloch wall)} \tag{48}$$

$$\alpha = \frac{2\, \mu_0\, \Delta\chi}{\gamma_1}\, H_0^2, \quad \beta = \frac{2\, K_{33}}{\gamma_1\, \rho_0^2}, \quad \delta = 1 - \frac{K_{11}}{K_{33}}. \qquad \text{(Néel wall)} \tag{49}$$

In (47) $\gamma(\nu, x)$ stands for the incomplete Gamma function, whose integral representation is

$$\gamma(\nu, x) = \int_0^x \mathrm{d}t\, \mathrm{e}^{-t}\, t^{\nu-1}. \tag{50}$$

From the solution for the auxiliary variable $\tilde{a}(t)$ the time evolution of the wall half-width $\xi_0(t)$ is obtained by simple back substitution,

$$\xi_0(t) = \frac{3\pi}{4a(t)} = \frac{3\pi}{4}\sqrt{\tilde{a}(t)}. \tag{51}$$

IV. QUANTITATIVE RESULTS

The analytical results for the dynamics of cylindrical domain walls in nematics that have been obtained in the previous section can be specified to real materials. For further considerations we choose the parameters that enter the solutions according to the nematic phase of PAA (p-azoxyanisole) at 120°C [1,2] (Table I).

splay elastic constant K_{11}	$7.0 \cdot 10^{-12}$ N
twist elastic constant K_{22}	$4.3 \cdot 10^{-12}$ N
bend elastic constant K_{33}	$1.7 \cdot 10^{-11}$ N
rotational viscosity γ_1	$6.7 \cdot 10^{-3}$ Nm/s
magnetic anisotropy $\mu_0\,\Delta\chi$	$1.21 \cdot 10^{-7}$

TABLE I: Material constants of PAA at 120°C.

The magnetic field strength H_0 has been chosen 500 Oersted, according to a magnetic flux density $B_0 \equiv \mu_0\, H_0 = 0.05$ T.

The initial configuration is a cylindrical domain wall at rest. At zero time the cylinder radius is by two or three orders of magnitude larger than the wall half-width: $\rho_0 \equiv \rho(t = 0) = 0.1\,\mathrm{mm}$, with $\tilde{\xi}_0 \equiv \xi_0(t = 0) = 1\,\mu\mathrm{m}$ or $0.1\,\mu\mathrm{m}$.

Fig. 3 shows the shrinking of the wall according to the square-root law (35), (36). The actual decay time is the moment when the cylinder radius touches the edge of the wall. However, from the temporal evolution of the wall width (see below) it is obvious that the decay time is only slightly overestimated when taking the time for which the cylinder has shrinked to zero.

$$\tau_{\text{decay}} = \frac{\gamma_1\, \rho_0^2}{2\, K_{22}}, \qquad \text{(Bloch wall)} \tag{52}$$

$$\tau_{\text{decay}} = \frac{\gamma_1\, \rho_0^2}{2\, K_{33}}. \qquad \text{(Néel wall)} \tag{53}$$

The main feature of the Bloch wall are twist deformations, whereas the Néel wall rather consists of bend deformations. The decay times (52), (53) depend on the elastic constants K_{33} and K_{22}: the Néel wall decays about four times faster than the Bloch wall.

Interestingly, the dynamics of the wall width reveals two separated processes on different time scales. First a rapid change occurs from the initial half-width to a metastable state that does not depend on the initial condition (Figs. 4 and 5). The metastable half-width can be related to the magnetic coherence length ξ_{mag}. For planar geometry the director would reorient in an external magnetic field by a *twist* deformation on a length scale [19] of

$$\xi_{\text{mag}} = \sqrt{\frac{K_{22}}{\mu_0\, \Delta\chi}}\, \frac{1}{H_0} \tag{54}$$

Introducing the parameters given at the beginning of this section, we obtain $\xi_{\text{mag}} = 0.15\,\mu$m for the half-width of a planar Bloch wall. However, according to Figs. 4 and 5 the metastable value for the half-width of the cylindrical Bloch wall is $\xi_{\text{Bloch}} = 0.21\,\mu$m. The discrepancy is due to the curvature that gives rise to additional *bend* deformations. Assuming that a similar law as Eq. (54) also holds for the curved wall, we can extract an effective elastic constant $K_{\text{Bloch}} = 8.4 \cdot 10^{-12}$ N. For the curved Néel wall the coherence length (Figs. 4 and 5) is $\xi_{\text{Neel}} = 0.68\,\mu$m, corresponding to an effective elastic constant of $K_{\text{Neel}} = 8.85 \cdot 10^{-11}$ N. This means that the elastic energy content of cylindrical domain walls is about one order of magnitude larger for the Néel geometry as compared to the Bloch-like reorientation.

As already stated above the effective coherence length ξ_{Bloch} or ξ_{Neel} denotes a metastable state. After some seconds, when the cylinder has shrinked so that its radius $\rho(t)$ is of the order $\xi_0(t)$, our solution for the wall half-width breaks down. Formally, our expressions for the Bloch wall reveal an implosion (Fig. 6), whereas for the Néel wall we obtain an explosion (Fig. 7) of the wall width. This is due to the opposite sign of the quantity δ in (46) and (47) and thus depending on the relative magnitude of the elastic constants (*cf.* (48), (49)).

Actually, one should remember that for wall half-widths larger than the cylinder radius the boundary conditions (24) are not correct, and then our solutions loose their physical meaning. Thus, within the framework of the polynomial expansion we are able to study the decay of the cylindrical domain wall until its radius becomes approximately equal to its half-width.

V. REMARKS

1. Our solutions for $\rho(t)$ and $\xi_0(t)$ give a rather detailed description of the time evolution of cylindrical domain walls. First of all, it would be interesting to compare our theoretical predictions with experimental results. Furthermore, because our expressions explicitly show how the dynamics of the domain wall depends on the material constants K_{11}, K_{22}, K_{33}, μ_0 and γ_1, they could be useful for the determination of these constants by observing the shrinking of the cylindrical domain walls.

2. It is possible to generalize our calculations to domain walls of a more general shapes, *e.g.* we could allow for a modulation along the z-axis or for non-circular sections by the x-y-plane. For the relativistic scalar field theory this has been performed in the second of the references [13]. The calculations in the general case the are much more cumbersome than for strictly cylindrical symmetry, while the main ideas of the polynomial approximation remain unchanged. For this reason we have chosen to restrict our presentation to the cylindrical geometry.

ACKNOWLEDGMENTS

As a Feodor-Lynen fellow J. S. gratefully acknowledges his individual grant from the Alexander von Humboldt-Stiftung.

REFERENCES

[1] S. Chandrasekhar, Liquid Crystals, Cambridge University Press, Cambridge (1992).

[2] P. G. de Gennes, The Physics of Liquid Crystals, Clarendon Press, Oxford (1993).

[3] M. Kléman, Points, Lines and Walls, Wiley, Chichester (1983).

[4] Y. Ouchi, H. Takezoe, A. Fukuda, Jap. Jour. App. Phys. **26**(1), 1 (1987).

[5] Y. Yamada, T. Tsuge, N. Yamamoto, M. Yamawaki, H. Orihara, Y. Ishibashi, Ferroelectrics **84**, 123 (1988).

[6] J. E. Maclennan, Q. Jiang, N. A. Clark, Phys. Rev. **E 52**(4), 3904 (1995).

[7] Th. Seitz, J. Stelzer, H.-R. Trebin, J. Appl. Phys. **80**(3), 1381 (1996).

[8] J. Nehring, A. Saupe, J. Chem. Soc. Faraday Trans. II **68**, 1 (1972).

[9] W. Helfrich, Phys. Rev. Lett. **21**(22), 1518 (1968).

[10] C. Kittel, J. K. Galt, Solid State Phys. **3**, 439 (1956).

[11] F. Bloch, Z. Physik, **74**, 295 (1932).

[12] L. Néel, J. Phys. Radium **17**, 250 (1956).

[13] H. Arodź, A. L. Larsen, Phys. Rev. **D 49**, 4154 (1994); H. Arodź, Phys. Rev. **D 52**, 1082 (1995).

[14] J. L. Ericksen, Arch. Rational Mech. Anal. **4**, 231 (1960); Trans. Soc. Rheol. **5**, 23 (1961).

[15] F. M. Leslie, Quart. J. Mech. Appl. Math. **19**, 357 (1966); Arch. Rational Mech. Anal. **28**, 265 (1968).

[16] C. W. Oseen, Trans. Faraday Soc. **29**, 883 (1933).

[17] H. Zöcher, Trans. Faraday Soc. **29**, 945 (1933).

[18] F. C. Frank, Disc. Faraday Soc. **25**, 19 (1958).

[19] P. G. de Gennes, Mol. Cryst. Liq. Cryst. **12**, 193 (1971).

FIGURES

FIG. 1. Geometry and coordinates for a cylindrical Bloch wall. Projection onto a plane perpendicular to the cylinder axis.

FIG. 2. Geometry and coordinates for a cylindrical Néel wall. Projection onto a plane perpendicular to the cylinder axis.

FIG. 3. Temporal evolution of the radius of a cylindrical domain wall in PAA at 120°C. Initial wall radius $\rho(t=0) = 0.1\,\mathrm{mm}$. Solid: Bloch wall, dashed: Néel wall.

FIG. 4. Temporal evolution of the half-width of a cylindrical domain wall in PAA at 120°C. Initial wall half-width $\rho(t=0) = 1\,\mu\mathrm{m}$. Solid: Bloch wall, dashed: Néel wall.

FIG. 5. Temporal evolution of the half-width of a cylindrical domain wall in PAA at 120°C. Initial wall half-width $\rho(t=0) = 0.1\,\mu\mathrm{m}$. Solid: Bloch wall, dashed: Néel wall.

FIG. 6. Catastrophic behaviour of the width of a cylindrical Bloch wall in PAA at 120°C.

FIG. 7. Catastrophic behaviour of the width of a cylindrical Néel wall in PAA at 120°C.

J. Stelzer, H. Arodź: Figure 1

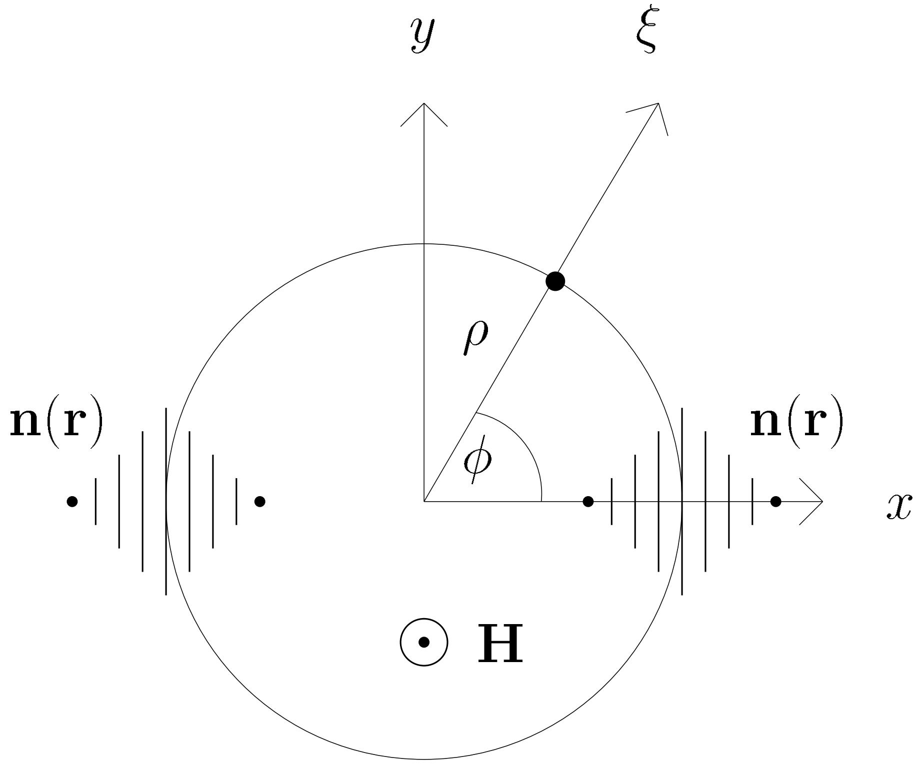

J. Stelzer, H. Arodź: Figure 2

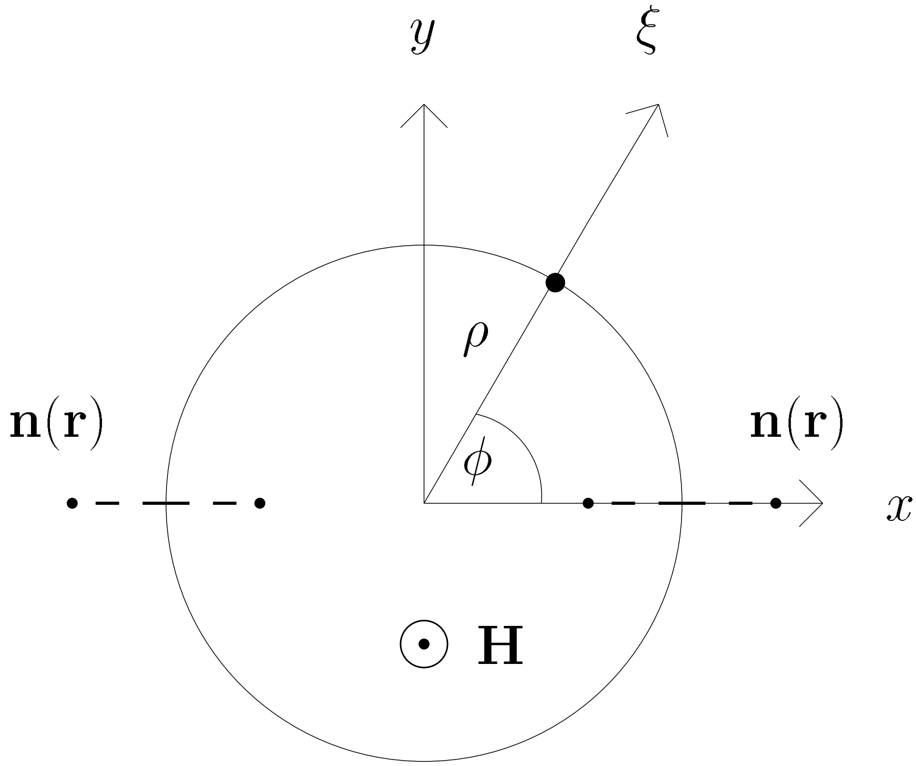

J. Stelzer, H. Arodź: Figure 3

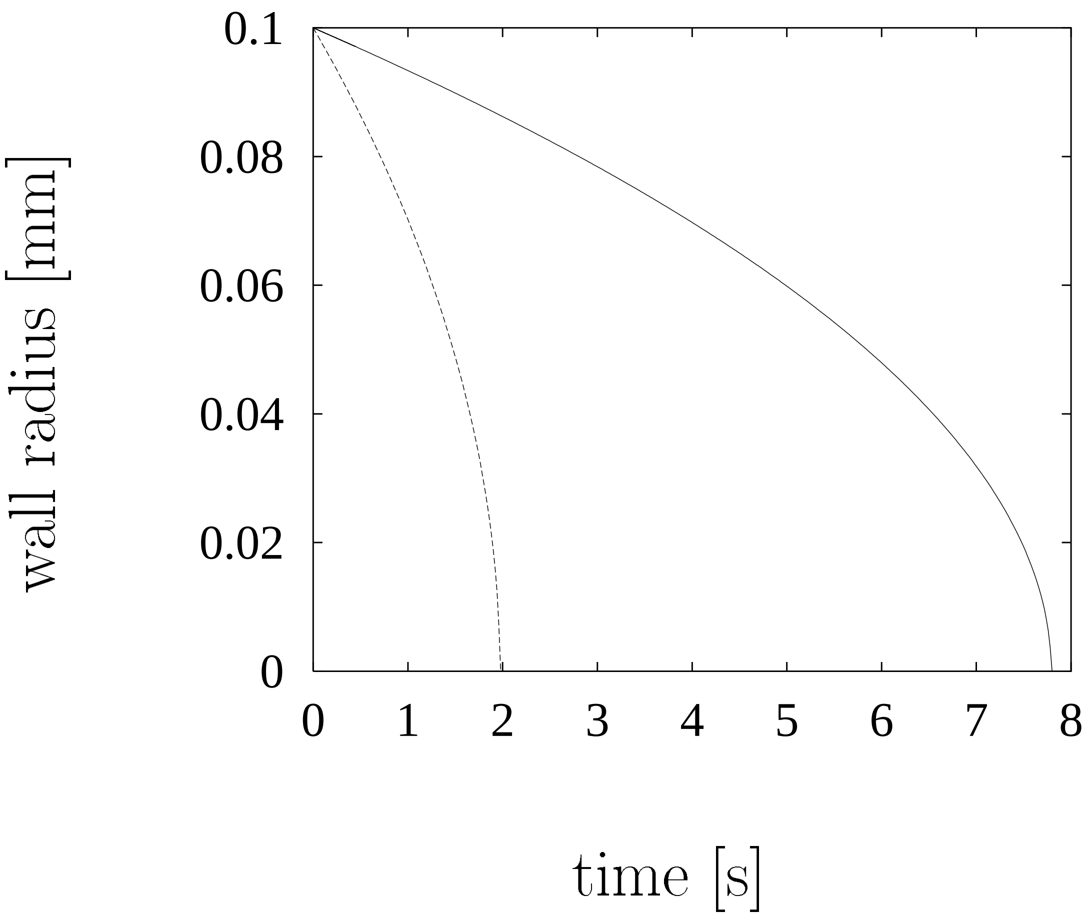

J. Stelzer, H. Arodź: Figure 4

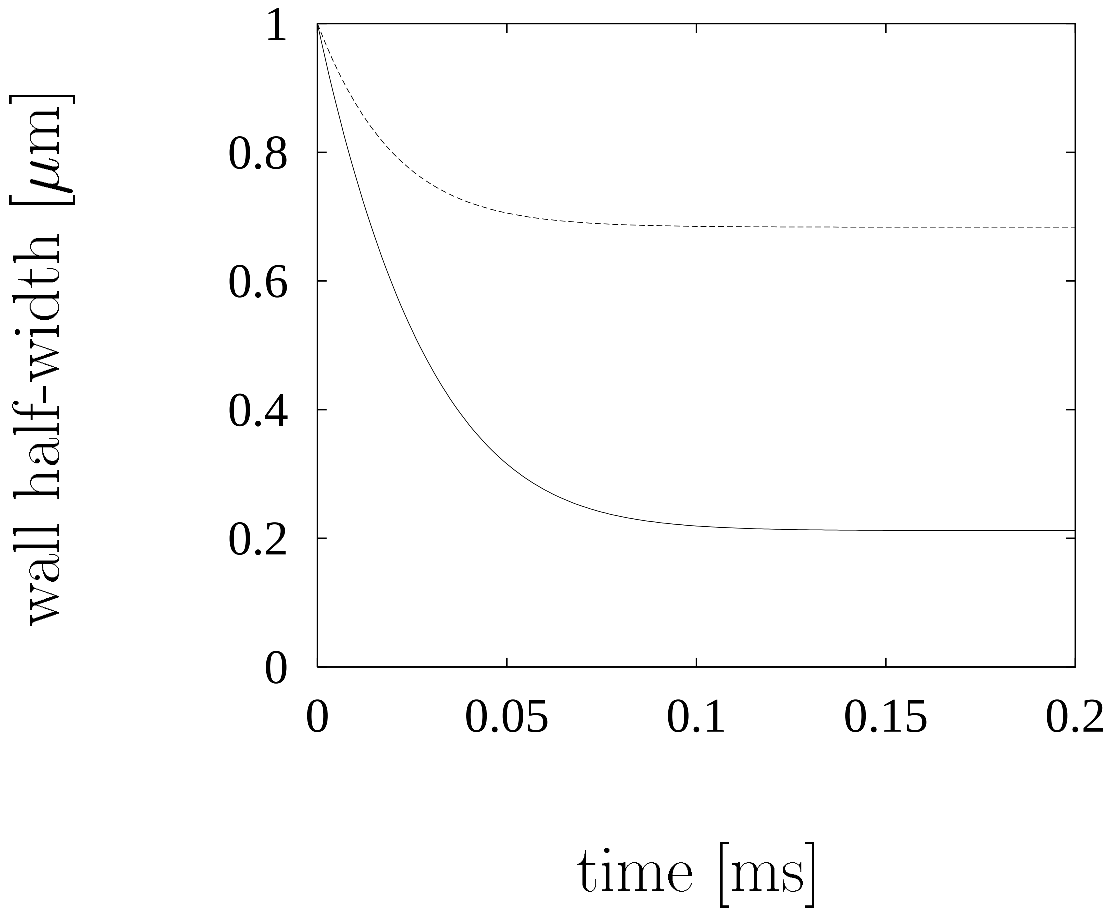

J. Stelzer, H. Arodź: Figure 5

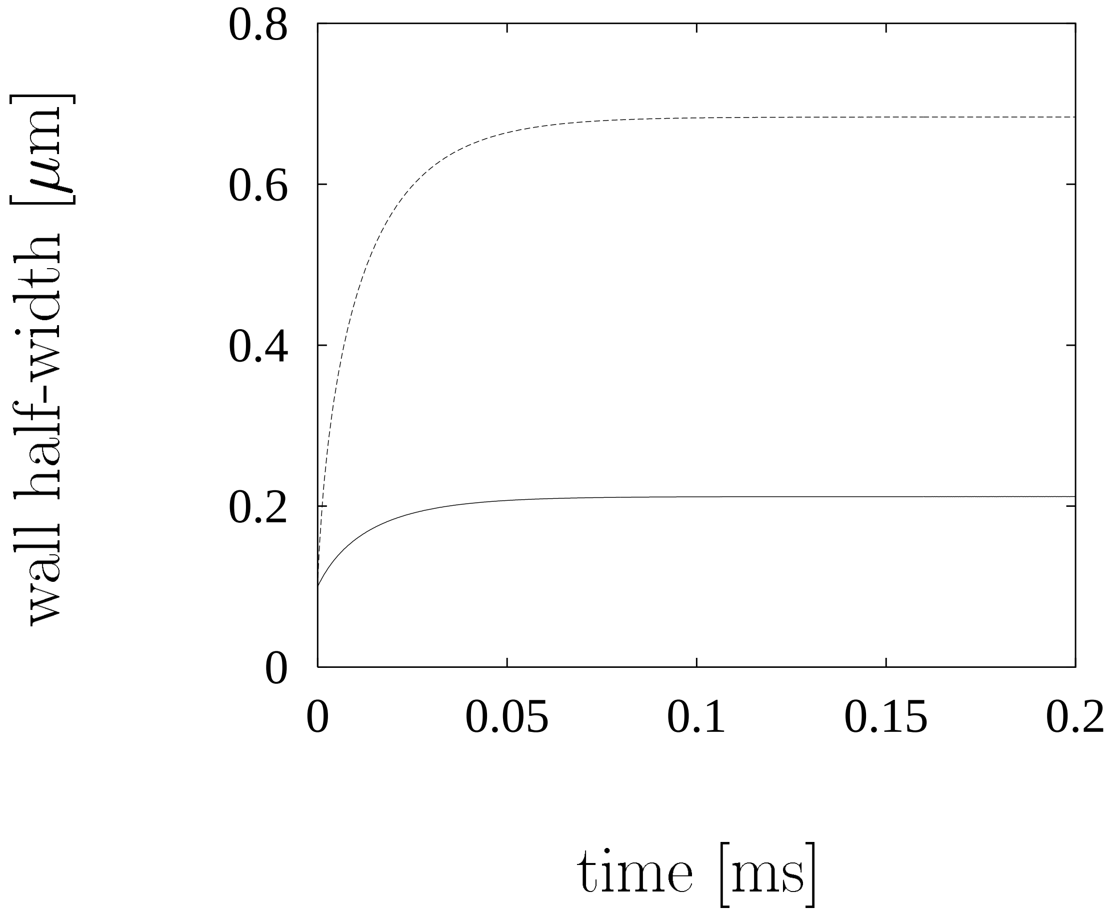

J. Stelzer, H. Arodź: Figure 6

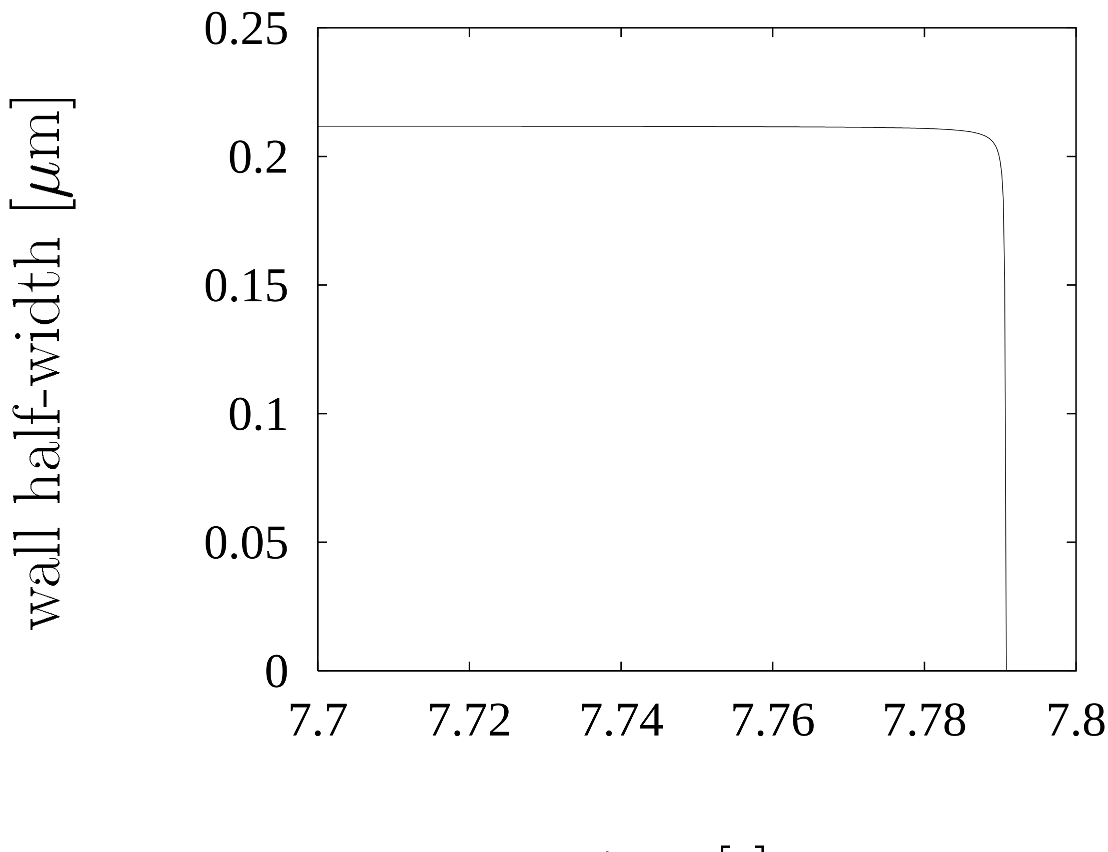

J. Stelzer, H. Arodź: Figure 7